IEEE Access
Multidisciplinary ⋮ Rapid Review ⋮ Open Access Journal

Received December 4, 2020, accepted January 7, 2021, date of publication January 21, 2021, date of current version January 29, 2021.

Digital Object Identifier 10.1109/ACCESS.2021.3053356

On-Line Precision Calibration of Mobile Manipulators Based on the Multi-Level Measurement Strategy

SHENG JIAN[1], XIANSHENG YANG[1], (Graduate Student Member, IEEE), XIANWEI YUAN[1], YUNJIANG LOU[1], (Senior Member, IEEE), YAO JIANG[2], GENLIANG CHEN[3], (Member, IEEE), AND GUOYUAN LIANG[4], (Member, IEEE)

[1]School of Mechatronics Engineering and Automation, Harbin Institute of Technology (Shenzhen), Shenzhen 518055, China
[2]Department of Mechanical Engineering, Institute of Manufacturing Engineering, Tsinghua University, Beijing 100084, China
[3]State Key Laboratory of Mechanical System and Vibration, Shanghai Jiao Tong University, Shanghai 200240, China
[4]Center for Intelligent and Biomimetic Systems, Shenzhen Institute of Advanced Technology, Chinese Academy of Sciences, Shenzhen 518055, China

Corresponding author: Yunjiang Lou (louyj@hit.edu.cn)

This work was supported in part by the National Natural Science Foundation of China (NSFC)-Shenzhen Robotics Basic Research Center Program under Grant U1713202, and in part by the Shenzhen Science and Technology Program under Grant JCYJ20180508152226630.

ABSTRACT Autonomous industrial mobile manipulator (AIMM), which is composed of a mobile platform and a robot arm of six degrees of freedom (DoFs), can move autonomously and perform dexterous tasks independently in the industrial environment. A novel on-line calibration system for AIMM in real manufacturing workshop is proposed in this paper. Compared to calibration scenarios of fixed-base robot, we focus on the large-space autonomous calibration for AIMM. To cope with the issue of high precision calibration in large space, we propose a multi-level guided-based measurement strategy, which includes the low-cost vision positioning and guidance system, and the high-precision distributed base station (BS) measurement system. The corresponding experiment proves that the total uncertainty of measurement system is less than 0.1 mm. Based on the measured data of end-effector installed at the end of robot arm, the AIMM can perform on-line calibration tasks anywhere automatically without taking into account the expensive devices for the high-precision location of mobile platform and the downtime for the robotic off-line calibration. The mean positioning error of AIMM after calibration reduces 93% based on the calibration experiment.

INDEX TERMS On-line robot calibration, base station, multi-level measurement strategy.

I. INTRODUCTION

Manufacturing problem of the large components, such as aircraft skins, space capsules, and carriage bodies of high-speed train, has become growing hot topic for related industry corporations or organizations [1]–[3]. Recently, the AIMM is gradually becoming the potential production equipment employed in large components manufacturing because of the features of dexterity, mobility and autonomous operations.

Due to the overall machining accuracy of large component is important in the manufacturing process, we are more concerned with the on-site absolute positioning accuracy of end-effector of the AIMM. Unfortunately, the AIMM does not possess the high-precision absolute positioning characteristics without any auxiliary facilities. Survey [4] indicates the reason comes from two aspects: 1) The accuracy of robot arm is inevitably affected by factors such as machining and assembly errors. 2) The mobile platform is rarely able to achieve the desired destinations due to the inherent low movement accuracy of mobile platform. To ensure the positioning accuracy of AIMM, the current solution is the so called ''offline calibration + real-time positioning''. That is, before the AIMM enters the work space, external pose measurement equipment (such as laser tracker and theodolite, etc.) is used to calibrate the robot arm in off-line mode (note that the geometric relationship between the mobile platform and the robot arm must be calibrated at the same time), then the pose of end-effector need to be determined in real-time when the AIMM is moving/operating in the work space.

The associate editor coordinating the review of this manuscript and approving it for publication was Hui Xie.

Although the solution of ''real-time positioning + offline calibration'' is a practical approach for the AIMM, there is still exist the following defects when the process of positioning and calibration are separated.

- **High-precision Requirements for Positioning Equipment.** The need of high precision measurement has a natural contradiction with the large space measurement [5]. The current global measuring equipment, such as vision camera and laser measuring equipment, have a decreasing relationship between the measurement accuracy and the measurement distance, so it is often costly to achieve high precision in a large space. On the other hand, if a global or distributed positioning device is used to directly position the end-effector (such as a commonly used visual servo solution) in real time, the workspace of end-effector will be constrained for avoiding the occlusion of the positioning signal during the movement of the robot arm [4].
- **Propagation of Positioning Error.** If a global or distributed positioning device is used to locate the mobile platform, the positioning error of mobile platform is transmitted to the base coordinate system of the robot arm [6], [7], and then to the end effector, making it difficult to achieve high-precision machining of the end effector. This is similar to the robot whose base is fixed, it is necessary to calibrate the base [8] with respect to the workstation.
- **The Inefficiency of Off-line Calibration.** At present, the off-line calibration schemes based on external sensors are mainly used to calibrate the manipulator and the relationship between the base of manipulator and the mobile platform. Off-line calibration is generally dependent on manual assistance, such as installing of calibration instruments and setting calibration configurations and measurement programs, which is a time-consuming and laborious process [9], [10].

This paper presents a novel on-line calibration system to improve the accuracy of the end-effector. Compared with the existing ''real-time positioning + offline calibration'' solution, the proposed solution abandons the strategy of using global or distributed measurement sensors to locate the robot, but directly adopts the on-site automatic calibration to achieve the same accuracy as the calibrated fixed mechanical arm in a large work space. Specifically, the proposed method is that the AIMM can be calibrated not only the kinematic parameters but also the operating relationship between the large component with the AIMM, that is, the localization error and the parameter error are eliminated synchronously by optimum fitting method. While the existing location method will either have to adopt the expensive positioning equipment (several hundred thousand dollars [5], [11]), or it will tolerate the relatively big error in type of self-localization model (the achievable position accuracy 5mm of KMR Quantic mobile-robot [4]). The main contributions of our calibration system as follow:

(1) The on-line calibration method proposed in this paper does not require the pre-calibration of the robot arm, but collecting the pose data and calibrating the total kinematic parameter during the operation of AIMM. Therefore, the calibration can start at the processing position.

(2) The distributed base station proposed can ensure a very high accuracy of measurement nearby the base station. Compared with the existing distributed measurement network (such as iGPS), it avoids the high cost of locating over the whole large space, but can meet the need of high-precision calibration near the processing position.

(3) By directly measuring the TCP (tool centre point) of the robot arm with multiple configurations to determine 1) the transformation relationship between the base coordinate system of the robot arm and the world coordinate system, 2) the kinematic geometric parameters and 3) the relationship between TCP coordinate system and flange coordinate system, that the positioning error of the mobile platform will not be transmitted to the end-effector of the robot arm.

(4) A multi-level guided system is introduced in this paper to help the measurement system (base station) automatically to realize the measurement task (the measurement task is the most time-consuming part in the calibration process). The guidance system is consist of low-cost infrared and optical cameras, which replaces the manual role in the traditional off-line calibration.

In the remainder of this paper, the problem statement for the calibration system is formulated firstly. Second, the model of measurement and guidance for AIMM applied in large space workshop is proposed. Third, a complete calibration modeling of the mobile manipulator is described. Finally, experiments prove the high precision of measuring network and feasibility of the total calibration system with real geometrical parameters.

II. RELATED WORKS

To improve the operation accuracy of robot, many researches have devoted into the research of kinematics off-line calibration. The process for model-based kinematics calibration generally includes four steps: kinematics modeling, end-effector pose measurement, parameters identification and error compensation. Hayati [12] proposed an improved DH (Denavit-Hartenberg) method to estimate the link parameter errors, which described the deviation between two adjacent parallel joints axes with an additional rotation transformation around y-axis. Chen [13] presented an analytical approach to determine the serial robot kinematic identifiable parameters based on the POEs (product of exponentials) formula. The imperfection of measuring device and identification algorithm can reduce the accuracy of the parameters. Quite a few researches are mainly concentrated on the measurement of position and orientation of robotic end-effector applying various measuring devices or multi-sensor integration, such as laser tracker, coordinate measuring instrument, theodolite and visual measuring system, etc. [14]–[17]. In algorithm ways, Nguyen [18] used an extended kalman filtering (EKF)

to identify robotic geometric parameters and an artificial neural network (ANN) to compensate the non-geometric error sources (such as the link deflection errors, joint compliance errors, gear backlash, etc.). [19], [20] presented the nonlinear optimization method for identifying the dynamic allowed load with flexible links or elastic links.

The real-time localization of mobile manipulator is another research hotspot in last few years [11], [21], [22], which along with the off-line calibration form the ''real-time positioning + offline calibration'' solution. The existed localization methods of AIMM are possible to classify into three classes: direct method, indirect method and self-localization method [4]. The direct method is to locate the end-effector by a global sensor. Norman *et al.* used the indoor GPS (iGPS) technology as an external measurement system to locate the receiver installed at end of robot arm [23]. The indirect method is to locate the mobile platform, where a transfer station is required to relate the mobile platform with the base of robot arm. Susemihl *et al.* presented an indirect locating approach for mobile manipulator in the large aircraft components machining applications, where a laser tracker with spherically-mounted reflectors (SMRs) at the mobile platform is required to locate the global position of mobile platform, and the stereo camera system (installed at the mobile platform) traces the absolute pose of the end-effector of the robot arm [24]. The self-localization is widely studied in the past couple of years, Borenstein *et al.* [25] surveyed relative literatures about the self-localization, and introduced four widely used methods including wheel odometry, inertial navigation, active beacons, landmark navigation, none of these approaches using external sensors.

Recently, some scholars have studied the on-line calibration methods based on the fixed-base robot. Compared with off-line approaches, the on-line approaches can obtain the measuring information and identify the actual kinematic parameters on-site, without shutdown the robot. Du *et al.* presented an on-line robot self-calibration method based on an inertial measurement unit (IMU) and a position sensor, which can obtain the real-time pose of EE and identify the parameters via extended kalman and particle filters [26]. The vision-based on-line calibration method in [10] was utilized to calibrate the robot itself kinematics parameters and the hand-eye relationship simultaneously in a robot-based inspecting system. An effective kinematic self-calibration method for dual-manipulators is presented to estimate the actual kinematic parameters in [27]. The on-line self-calibration approaches mentioned significantly improve the efficiency and accuracy of calibration, but the calibrated objects are still fixed-base robots rather than the AIMM with a mobile platform. Therefore, it needs to develop a high-accuracy on-line calibration approach for AIMM applied in large space workshops, but there has been relatively little work in this situation.

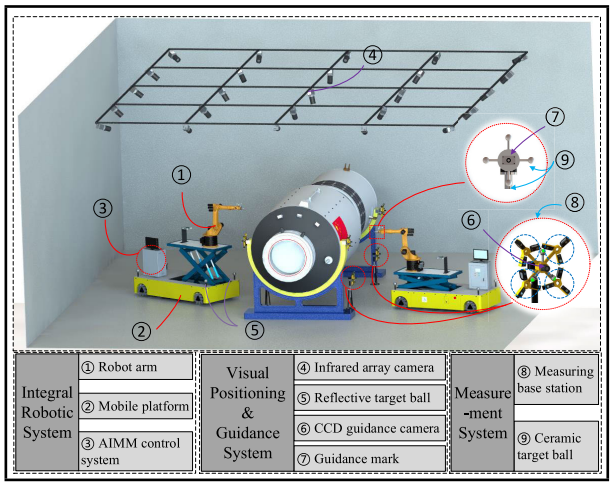

FIGURE 1. AIMM calibration system for machining scene.

III. PROBLEM STATEMENT

A. STRUCTURE FOR ON-LINE CALIBRATION

The proposed system is composed of the following three subsystems, and the scene graph is shown in Fig. 1.

(i) *Vision Positioning and Guidance System*
The vision positioning system, which includes the infrared array camera (IRAC) (④) and the reflective target balls ⑤ (installed on the mobile platform (②)), can locate the mobile platform with centimeter-lever accuracy. On the other hand, CCD camera with the millimeter-level resolution (⑥) is employed to recognize the guidance mark (⑦), which constitute the vision guidance system.

(ii) *Distributed Base Station Measurement System*
The distributed measurement system comprises multiple BSs (⑧) with micrometer-level accuracy, which are deployed anywhere on demand. A group of ceramic targets (⑨) is mounted on the flange of the robot arm. What's more, the CCD cameras are fastened to the center of BS in order to guide the robot arm to arrive measurable area in front of the base station.

(iii) *Robotic System*
A 6-DoF standard industrial robot arm (①) is installed on the upper interface of the mobile platform. The end-effector is equipped on the flange of the robot arm in order to perform certain machining tasks.

The entire process of the proposed method is shown in Fig. 2, in which 4 steps: kinematic modeling, end-effector pose measurement, parameter identification and compensation for kinematics parameters are included. [28] presented the trend of new generations of large-scale dimensional metrology (LSDM), it seems oriented towards the distributed system. Similarly, we design a distributed measurement system and each measurement node is called as ''measurement base station''. The measurement base station is a non-contact pose measurement device which is composed of several high-precision laser displacement measurement units. Since the

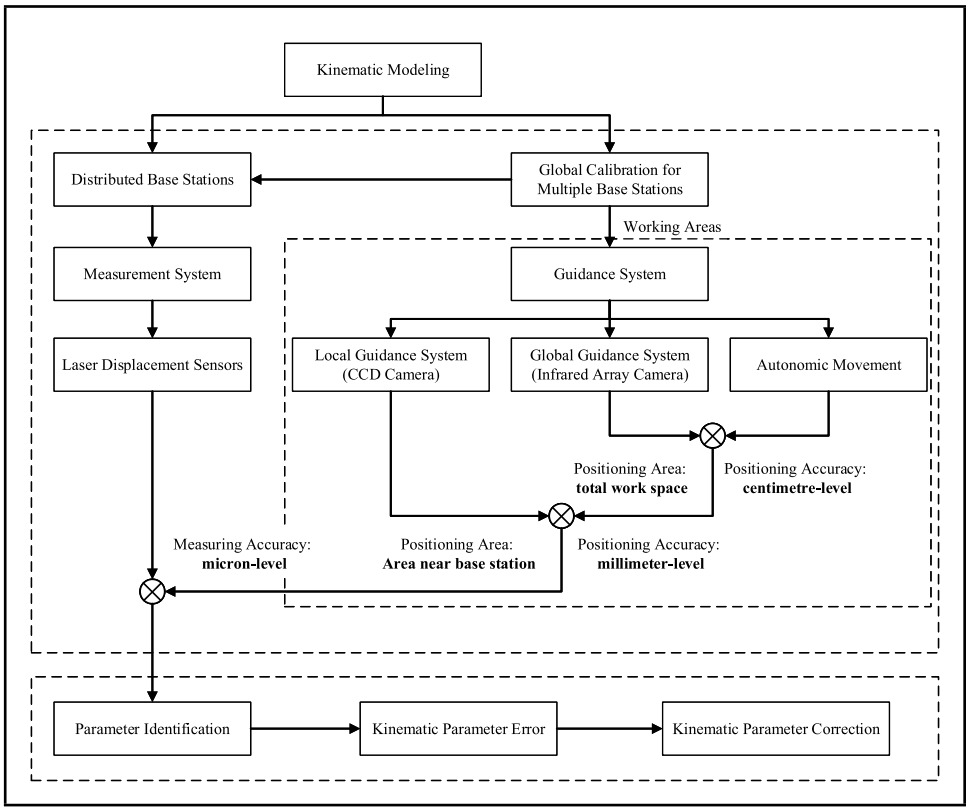

FIGURE 2. The framework for on-line calibration.

base station is deployed on demand in a large-scale space, it is necessary to calibrate the pose relationship of the multiple base stations in advance. Compared with a single global measurement device (such as a laser tracker), the distributed measurement network has strong scalability and is robust to solve occlusion problem of the measured target during the measurement process.

Furthermore, we introduce an autonomous multi-level guidance system [29], [30] to implement more efficient automatic pose estimation during the on-line calibration. In the article, the global large-space guidance system uses a low-cost infrared camera array (the spatial pose of the mobile platform can be positioned within centimeters), and the local guidance system uses the CCD camera (the spatial pose of the end-effector can be positioned within millimeters). These two-level guidance system greatly reduces the burden of the measurement system to search for the target (installed at the end-effector), and realizes automatic and rapid measurement. Therefore, the step-by-step guidance mechanism is a low cost and high efficiency auxiliary measuring equipment, which takes full account of the actual needs of high-precision calibration in a large space and replaces the manual role in the traditional off-line calibration.

B. DEFINE OF COORDINATE SYSTEM

To further formulate the operational details of the calibration, a coordinate transform relationship of the calibration system is presented in Fig. 3. At first, the frames of each part of the system are established as follows:

$\{W\}$: The *world frame* is the reference coordinate system in the workshop, and it is often set according to the standard reference.

$\{I\}$: The origin of *infrared camera frame* is assumed as the center point of the front lens of one camera in the IRAC. Moreover, the relationship between other cameras in the IRAC and this camera needs to be determined with the calibration tools given by vendor.

$\{M\}$: The *manipulator frame* is located on the base of robot arm.

$\{B_i\}$: The *base station frame* is located at *ith* base station, which determines the pose of the base station. The station frame is defined relative to the world frame, and the transfer matrix can be expressed as $\{B_i\} = {}^{W}_{Bi}T$.

$\{F\}$: The *flange frame* is fixed with the flange of manipulator.

$\{E\}$: The *end-effector frame* is located at TCP of the manipulator. In general, the homogeneous transformation ${}^{F}_{E}T$ is constant and can be pre-defined (not accuracy).

C. TOTAL CALIBRATION SCHEME

When entering the large-space work area, the AIMM always has two operating modes: driving mode and machining mode, which are described in [24]. In driving mode, the mobile platform moves to the predefined working area (BSs are often

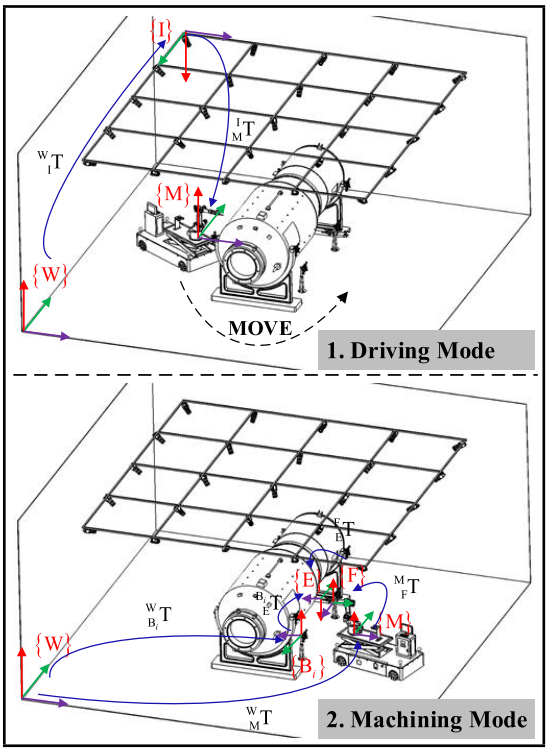

FIGURE 3. The coordinate transform relationship of calibration system.

set up nearby the working area). Then, the visual positioning system captures the pose (centimeter-level accuracy) of the mobile platform in real time by recognizing the reflective target balls fixed on the platform. The initial and imprecise relationship between the manipulator frame and the world frame can be described by homogeneous transformation,

$$ {}^{W}_{M}T = {}^{I}_{M}T \cdot {}^{W}_{I}T \tag{1} $$

In machining mode, the AIMM reaches the working area. The platform is lowered and decoupled from the driving unit, which avoids the influences like gear backlash and elasticity of the drive unit. Then the EE of robot arm move to the vicinity of the BS based on the estimated transformation ${}^{W}_{M}T$. Once the CCD guidance camera catching the guidance mark attached to the EE, the guidance program will be triggered to guide the ceramic target moving to the measurable area of the BS. So that ${}^{Bi}_{E}T$ can be measured in real time by the displacement sensors installed on the BS and the corresponding ceramic targets. Furthermore, we can get the pose of EE under the reference coordinate system if we know the relationship between the base station and reference, ${}^{W}_{Bi}T$. On the other hand, the pose can also be obtained in another transformation, that is, transformation from the end-effector frame to the manipulator frame then to the world frame. The initial relationship ${}^{W}_{M}T$ is known according to the calculation in driving mode, and the relationship ${}^{M}_{E}T$ is calculable base on nominal kinematic parameters given by the user manual. Thus, the above relationship can be formulated as,

$$ {}^{W}_{M}T\,{}^{M}_{F}T\,{}^{F}_{E}T = {}^{W}_{Bi}T\,{}^{Bi}_{E}T \tag{2} $$

Ideally, Eq (2) represents an identical relationship for the measured pose and the calculated pose. However, the nominal values of geometric parameters are generally not equal to the actual values as well as the deviation in the ${}^{W}_{M}T$, there exists discrepancy between the measurements and calculations.

Therefore, the problem is now simplified as that of determining the transformation ${}^{W}_{Bi}T$, then estimating the actual geometric values in ${}^{M}_{E}T$ by using a complete robot calibration process. The transformation ${}^{W}_{Bi}T$ can be determined with the establishment of measurement system, which is described in the section IV. The kinematic modeling about robotic parameters and the process of calibration are illustrated in Section V.

IV. MEASUREMENT AND GUIDANCE FOR AIMM

Compared to base-fixed robot arms, it is more challenging to obtain the pose in the calibration process directly because of the large-scale workspace of the mobile manipulators. While the large-scale dimensional metrology (LSDM) [28], [31] is a popular research topic, the existing measurement systems are less likely to meet the features of accuracy, distance, occlusion conditions and cost simultaneously.

Considering that the operating areas of the mobile manipulators are often preset in the industrial structural environment, this section mainly describes the establishment of transformation ${}^{W}_{Bi}T$, which includes three parts: design of base station, global calibration of base station and vision-based guidance measurement.

A. DESIGN OF BASE STATION

The base station, as shown in Fig. 4, is composed of multiple sets of laser displacement measuring units. If three laser displacement sensors are set in one measuring unit, they are symmetrical separated by 120 degrees in this virtual circle. On account of the fixture is precisely machined, the pose transformation relation between each laser displacement sensor and the base station frame is known beforehand. In addition, the measurement tolerance of laser displacement sensor can be ignored due to the high-precision laser measurement and short measuring distance. Thus, the objective to get the high precision measurement of the base station near a specific can be achieved base on the two conditions above.

The main purpose of the BS is to measure the transformation i.e., ${}^{Bi}_{E}T$. Theoretically, the pose of the robot arm can be calculated by three sets of units (based on multi-lateration method [32]). An additional set of measurement unit is also used to improve the accuracy of the measurement and reliability. Moreover, the symmetrical structure is also able to ensure that each sensor in the base station will change in a proportional radial manner during the thermal deformation process.

B. GLOBAL CALIBRATION OF BASE STATION

In order to measure the EE of robot arm accurately with the help of base station, the transformation between the base station frame and the world frame must be determined. Laser

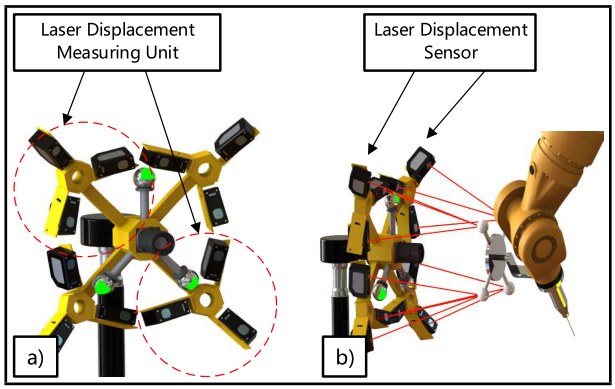

FIGURE 4. Base station of measurement system.

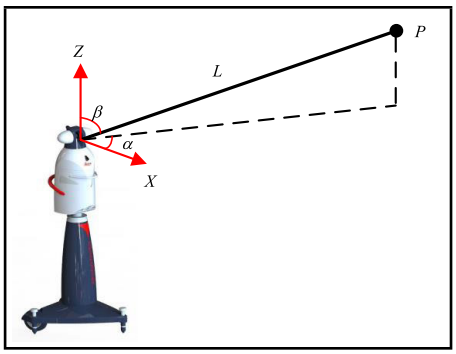

FIGURE 5. Laser tracker measurement principle.

tracker is an efficient large-scale 3D coordinate measurement instrument. The base station frame can be defined by measuring the central points of three SMRs (installed at the predefined non-colinear plane of the BS). As shown in Fig. 5, for calculating the position of the space point $P = (x\ y\ z)$, according to [33], laser tracker need to measure the radial length L relative to the measured origin and two spatial angles (horizontal angle α and vertical angle β),

$$\begin{cases} x = L\sin\beta\cos\alpha \\ y = L\sin\beta\sin\alpha \\ z = L\cos\beta \end{cases} \tag{3}$$

The measurement error of the laser tracker comes from distance measurement error and angle measurement error. To be more specific, compared with distance measurement of the laser interferometer (IFM), angle measurement accuracy is prone to lower due to the resolution of the motor encoder and adverse environmental factors, so the measurement error is mainly decided by angle measurement error [33]. Take Leica AT960 absolute laser tracker as an example, the uncertainty distance measurement module is less than $10\mu m$ in the full range. However, the angle measurement uncertainty can reach $15\mu m + 6\mu m/m$.

A 3D coordinate measurement approach referred to as the trilateration method [32] is utilized to solve the issues above. The approach abandons angle measurement and only based on IFM. Thus, four laser trackers with non-coplanar deployment are required to measure the absolute distance L

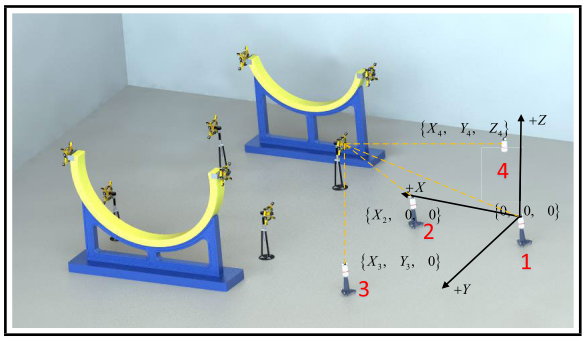

FIGURE 6. Spatial point position measurement by trilateration method.

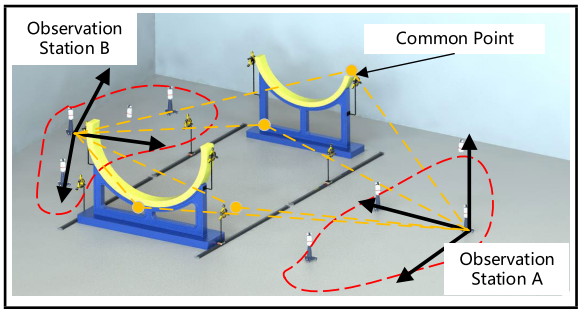

FIGURE 7. Point-based station-transfer measurement.

of one spatial point. As shown in Fig. 6, S_1, S_2, S_3 and S_4 represent the coordinate origin of laser beam emitter on laser trackers respectively. Then the 3D coordinates of point P can be determined if the distances from the measuring point P to the three origin points are accurately measured. Typically, if we know the coordinates of the three points and the distance to the unknown point, the following spherical equations can be established,

$$\begin{cases} (x - X_1)^2 + (y - Y_1)^2 + (z - Z_1)^2 = d_1^2 \\ (x - X_2)^2 + (y - Y_2)^2 + (z - Z_2)^2 = d_2^2 \\ (x - X_3)^2 + (y - Y_3)^2 + (z - Z_3)^2 = d_3^2 \end{cases} \tag{4}$$

The fourth laser tracker d_4 can be used for formulating the residual equation with $|S_4P|$

$$res = d_4 - \sqrt{(x - X_4)^2 + (y - Y_4)^2 + (z - Z_4)^2} \tag{5}$$

Each additional unknown point increase four residual equations and three unknown parameters $(x_i\ y_i\ z_i)\ i = 1, 2 \ldots n$. In addition, the 3D coordinate of these laser trackers are defined as $S_1 = \{0\ 0\ 0\}$, $S_2 = \{X_2\ 0\ 0\}$, $S_3 = \{X_3\ Y_3\ 0\}$ and $S_4 = \{X_4\ Y_4\ Z_4\}$ for convenience, and these constitute an observation station with six unknown parameters. In general, the number of unknown spatial is given by a simple formula points $4n \geq 6 + 3n$, and six measured points at least are needed to complete the self-calibration of observation station.

For multiple BSs in the large space, shown in Fig. 7, it is inevitable to encounter the situation that the light beam of the laser tracker would be blocked by the barriers, such as large parts or BS itself. The transformation between the BS frame

and the world frame can not be directly calibrated if the beam is blocked. A method based on point-based station-transfer is proposed to solve the issue. In the method, several SMRs (often are called as common points) would be randomly placed on the public area where two or more observation stations can observe these common points. The measured value of one common point is ${}^{A}Q_i = \left\{ {}^{A}x_i \ {}^{A}y_i \ {}^{A}z_i \right\}$ relative to observation station A coordinate system, and the measured value of the common point is ${}^{B}Q_i = \left\{ {}^{B}x_i \ {}^{B}y_i \ {}^{B}z_i \right\}$ relative to observation station B coordinate system. Thus, the orientation and position between station A and station B can be calculated with several common points,

$$ {}^{A}Q_i = {}^{A}_{B}R\,{}^{B}Q_i + {}^{A}_{B}t \tag{6} $$

C. STRATEGY OF VISION-BASED GUIDANCE

The end-effector of AIMM is particularly hard to enter directly into the measurable area of the base station because the area is relatively small. Therefore, a strategy of vision-based guidance that locates the AIMM in real time and guides the robot arm to seek for the appropriate measurable configuration automatically is proposed, the positioning accuracy of end-effector increases hierarchically, from cm-level to mm-level and then to micron-level. The former is achieved in driving mode, and the latter is done in machining mode.

During the driving mode, the co-viewing area (public view with at least two cameras) of the camera array must cover the entire workspace in order to position the mobile platform. We use a lower resolution camera because cm-level accuracy is generally sufficient to meet our requirements. On the other hand, as shown in Fig. 8, the calibration board installed at the pre-defined position of BS to determine the transformation relationship between the camera frame and the world frame. Since the transformation ${}^{W}_{Bi}T$ is calibrated in the previous section, each camera in camera array can search the BS in sight to calculate the exterior parameters automatically.

$$ {}^{W}_{C}T = {}^{W}_{B}T\,{}^{B}_{P}T\,{}^{P}_{C}T \tag{7} $$

According to rough location (previous step), the robot arm can move the end-effector into the field of view of the CCD camera, who is installed at the pre-defined location of the BS. As shown in Fig. 9, the resolution of the CCD camera is mm-level within 1 meter view distance. Then, the CCD camera extracts the center of the ring in the visual guidance marker and calculates the pose of the marker based on the known intrinsic parameters of the camera. When the controller of AIMM obtains the pose information of the marker by the CCD camera, the ceramic target (represents the end-effector of robot arm) is guided to the suitable pose (configuration) where all laser displacement measuring units can measure the target directly and get the distances between the laser emission point and the sphere surface.

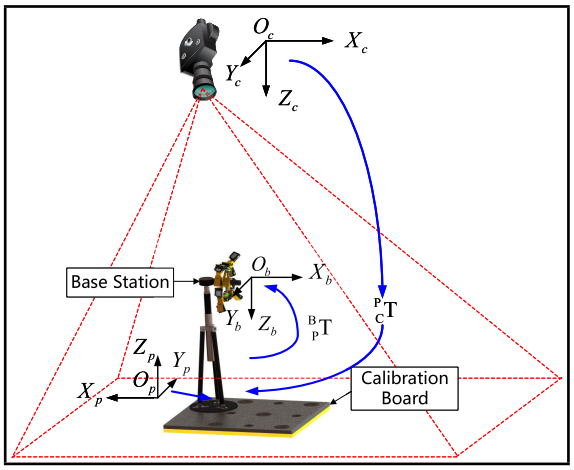

FIGURE 8. Calibration for exterior parameters of camera array.

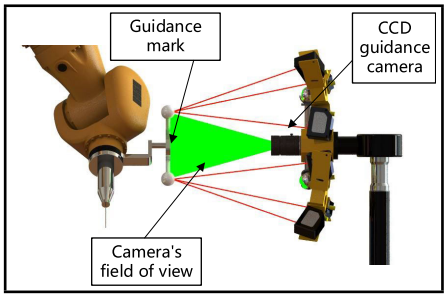

FIGURE 9. Vision-based guidance by CCD camera.

V. KINEMATIC CALIBRATION METHODOLOGY

Denavit-Hartenberg (DH) method is a popular modeling approach used for robotic kinematic calibration [34]. However, the differential error model base on DH method is discontinuous if the robot exists the adjacent parallel axes. Hayati's method in [12] is adopted in this article to establish the robotic kinematic model.

The homogeneous matrix ${}^{i}_{i+1}T$ represents transformation relationship of coordinate system $\{i+1\}$ relative to coordinate system $\{i\}$, in which the parameters θ_i, d_i, a_i, α_i and β_i are utilized to describe the homogeneous matrix and given by (8), as shown at the bottom of the page, where θ_i is the angle between X_i and X_{i+1} measured about Z_i, d_i is the distance between X_i and X_{i+1} measured about Z_i, α_i is the angle

$$ \begin{aligned} {}^{i}_{i+1}T &= rot\,(z,\theta_i)\,trans\,(0,0,d_i)\,rot\,(x,\alpha_i)\,trans\,(a_i,0,0)\,rot\,(y,\beta_i) \\ &= \begin{bmatrix} c\theta_i c\beta_i - s\theta_i s\alpha_i s\beta_i & -s\theta_i c\alpha_i & c\theta_i s\beta_i + s\theta_i s\alpha_i c\beta_i & a_i c\theta_i \\ s\theta_i c\beta_i + c\theta_i s\alpha_i s\beta_i & c\theta_i c\alpha_i & s\theta_i s\beta_i - c\theta_i s\alpha_i c\beta_i & a_i s\theta_i \\ -c\alpha_i s\beta_i & s\alpha_i & c\alpha_i c\beta_i & d_i \\ 0 & 0 & 0 & 1 \end{bmatrix} \end{aligned} \tag{8} $$

between Z_i and Z_{i+1} measured about X_{i+1}, a_i is the distance between Z_i and Z_{i+1} measured about X_{i+1}, β_i is the angle of rotation about Y_{i+1} when Z_i is almost parallel to Z_{i+1}. In addition, We use 6 parameters (3 translation parameters ${}^{w}d_x$, ${}^{w}d_y$, ${}^{w}d_z$ and 3 rotation parameters ${}^{w}\gamma_x$, ${}^{w}\gamma_y$, ${}^{w}\gamma_z$) to represent the transformation from base coordinate system of robot arm to the world coordinate system, ${}^{W}_{M}T$, and 3 parameters (${}^{e}d_x$, ${}^{e}d_y$, ${}^{e}d_z$) to represent the transformation from end-effector coordinate system of robot arm to the flange coordinate system, ${}^{E}_{F}T$. Thus, the relationship among those matrices are given by:

$$ {}^{W}_{E}T = {}^{W}_{M}T\,{}^{M}_{2}T\,{}^{2}_{3}T\,{}^{3}_{4}T\,{}^{4}_{5}T\,{}^{5}_{6}T\,{}^{6}_{F}T\,{}^{F}_{E}T = {}^{W}_{M}T\,{}^{M}_{F}T\,{}^{F}_{E}T \tag{9} $$

With the influence of parameter errors, the homogeneous matrix ${}^{i}_{i+1}T$ contains relevant deviation ${}^{i}_{i+1}\Delta T$. The kinematic differential error model based Eq (9) is established, which can be formulated with the linear perturbation method,

$$ {}^{W}_{E}T + {}^{W}_{E}\Delta T = \left({}^{W}_{M}T + {}^{W}_{M}\Delta T\right) \cdot \prod_{i=M}^{F}\left({}^{i}_{i+1}T + {}^{i}_{i+1}\Delta T\right) \cdot \left({}^{E}_{F}T + {}^{E}_{F}\Delta T\right) \tag{10} $$

Assume the higher order differential terms are ignored, and we only use the position data set to identify the kinematic parameters, Eq (10) is simplified as:

$$ {}^{W}_{E}\Delta p = {}^{W}_{M}\Delta T\,{}^{M}_{F}T\,{}^{F}_{E}p + {}^{W}_{M}T\,{}^{M}_{F}\Delta T\,{}^{F}_{E}p + {}^{W}_{M}T\,{}^{M}_{F}T\,{}^{F}_{E}\Delta p \tag{11} $$

To simplify identification procedure, we separate the calibration of linkage parameters (d_i, a_i, α_i and β_i) from the calibration of the world-base parameters (${}^{w}d_x$, ${}^{w}d_y$, ${}^{w}d_z$ and ${}^{w}\gamma_x$, ${}^{w}\gamma_y$, ${}^{w}\gamma_z$) and tool-flange parameters (${}^{e}d_x$, ${}^{e}d_y$, ${}^{e}d_z$), then the separated two calibration process will to be loop iteratively for several times.

Firstly, when we deal with the estimation of the world-base parameters and tool-flange parameters, the initial value of parameters are given by rough location (global visual positioning) and SolidWorks model of tool, respectively. Let X and Y be the unknown 4*4 homogeneous transformation ${}^{F}_{E}T$ and ${}^{W}_{M}T$, and let A_i and B_i represent the homogeneous transformation ${}^{W}_{E}T$ and ${}^{M}_{F}T$ under the i-th measured configuration. Thus, the issue of estimating world-base/tool-flange parameters simultaneously is converted to solve equation group $A_iX = YB_i$, where the solution has been proposed firstly in literature [35].

The second process is to estimate linkage parameters, where the results of the world-base parameters and tool-flange parameters in the process one are used. Set ΔT_i represents the differential transformation between the coordinate systems of two adjacent links, and derive the linear combination of linkage parametric errors:

$$ \Delta T_i = \frac{\partial T_i}{\partial \theta_i}\Delta\theta_i + \frac{\partial T_i}{\partial d_i}\Delta d_i + \frac{\partial T_i}{\partial \alpha_i}\Delta\alpha_i + \frac{\partial T_i}{\partial a_i}\Delta a_i + \frac{\partial T_i}{\partial \beta_i}\Delta\beta_i \tag{12} $$

where the $\Delta\theta_i$, Δd_i, $\Delta\alpha_i$, Δa_i and $\Delta\beta_i$ represent the small error of each link parameter based on Hayati's model. Combine Eq (8) and Eq (12), the differential transformation of the robot linkage $\{i\}$ and $\{i+1\}$ can be written in the following linear form:

$$ \begin{bmatrix} dx_i \\ dy_i \\ dz_i \\ \delta x_i \\ \delta y_i \\ \delta z_i \end{bmatrix} = \begin{bmatrix} 0 & 0 & -d_i s\theta_i & c\theta_i & a_i s\theta_i s\alpha_i - d_i c\theta_i c\alpha_i \\ 0 & 0 & d_i c\theta_i & s\theta_i & -a_i c\theta_i s\alpha_i - d_i s\theta_i c\alpha_i \\ 0 & 1 & 0 & 0 & ac\alpha_i \\ 0 & 0 & c\theta_i & 0 & -s\theta_i c\alpha_i \\ 0 & 0 & s\theta_i & 0 & c\theta_i c\alpha_i \\ 1 & 0 & 0 & 0 & s\alpha_i \end{bmatrix} \times \begin{bmatrix} \Delta\theta_i \\ \Delta d_i \\ \Delta\alpha_i \\ \Delta a_i \\ \Delta\beta_i \end{bmatrix} \tag{13} $$

Combine Eq (12) and Eq (13), the relationship between the position and orientation error (ΔX) of the robot arm flange with the link parameter errors (ΔK) can be simplified as linear parametric equations as $\Delta X = J_i \cdot \Delta K$, where the J_i is the Identification Jacobian Matrix of the link $\{i\}$ and $\{i+1\}$ in one measuring configuration. Note that the number of linear equation (a measuring configuration can provide 3 equations) needs to be greater (in general, 2∼3 times) than the number of parameters to be identified. Finally, we use the least square fitting method to solve the kinematic parameter errors $\Delta\theta_i$, Δd_i, $\Delta\alpha_i$, Δa_i and $\Delta\beta_i$, and update the nominal values of kinematic parameters with the parameter errors.

VI. EXPERIMENTS

A. UNCERTAINTY VERIFICATION OF MEASUREMENT SYSTEM

Since the measurement system is determined by the BSs distributed around the large space, it is essential to evaluate the pose accuracy of the BSs in advance. The process of verified experiment is presented as following steps and shown in Fig. 10:

STEP 1: In a space of 10m*10m*10m where large workpieces are placed, 4 laser trackers will be used to form an observation station (supposing it is called the observation station A) to determine the 3D positions of measurable SMRs installed at each base station. The reason for using multiple laser trackers is that we only use the length measurement information of the laser interference of the tracker to estimate the measured point. Meanwhile, the coordinate system of observing station A is estimated by the method described in Section IV(B).

STEP 2: If some SMRs is outside the field of view of the observation station, we will move the laser trackers to any position for forming a new observation station (supposing it is called the observation station B) so that these SMRs can be measured by new observation station.

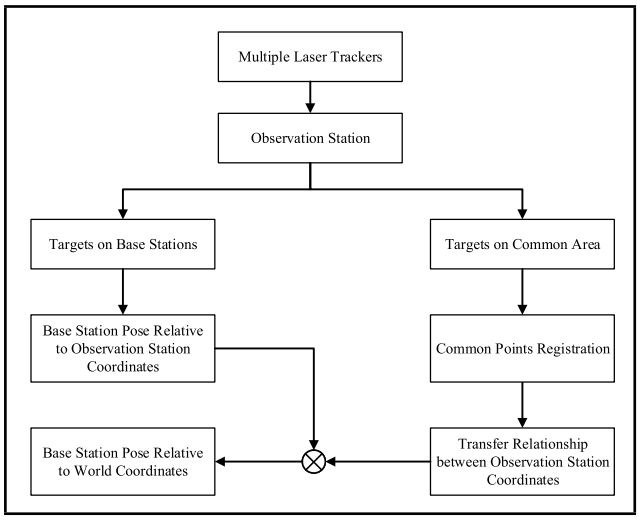

FIGURE 10. The global calibration process of measurement system.

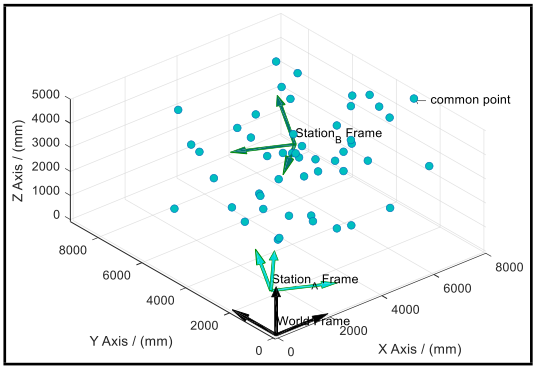

FIGURE 11. The distribution of common point and observation station.

STEP 3: 50 common points are deployed in the common field of view of multiple observation stations (observation station A and observation station B), which is shown in Fig. 11. The Levenberg-Marquardt (LM) algorithm is used to solve the transformation relationship of observation station frames base on the registration 25 of the common points. The other 25 common points are used to verify the accuracy of the transformation relationship.

STEP 4: Determine the representation of the base station coordinate system in the world (reference) coordinate system through the transformation relationship. If we assume the coordinate system of the observation station A is the reference coordinate system, then the mean position accuracy of the common points measured by observation station B (relative to the coordinate system of observing station A) is 0.0377mm. On the contrary, If we assume the coordinate system of the observation station B is the reference coordinate system, the mean position accuracy of the common points measured by observation station A (relative to the coordinate system of observing station B) is 0.0383mm. Error details in different reference frames (observation station A or B) is shown in Fig. 12. Meanwhile, the transformation between the

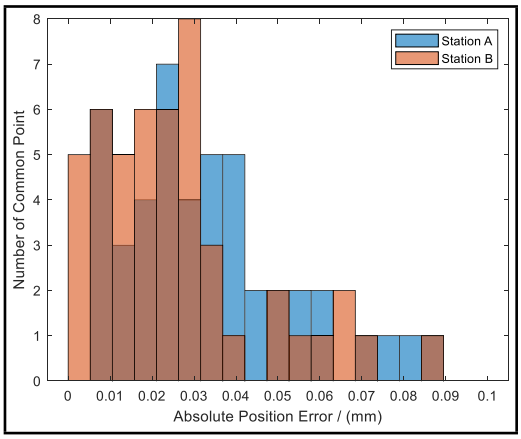

FIGURE 12. The absolute position error of common point observed by the station *A* and station *B*.

two station can be obtain:

$$
{}^{A}_{B}R = \begin{bmatrix} -0.4005 & -0.234 & -0.8859 \\ -0.8850 & 0.3491 & 0.3079 \\ 0.2372 & 0.9074 & -0.3469 \end{bmatrix},
$$
$$
{}^{A}_{B}t = \begin{bmatrix} 2817.427 \\ 8438.486 \\ -2020.100 \end{bmatrix} \tag{14}
$$

As several SMRs can be observed by different observation stations (base station coordinate system is established by 3 measurable SMRs), it can be inferred that the positioning uncertainty of base station can also be controlled within 0.05mm. At the same time, considering that the measurement accuracy of the laser displacement sensor inside the base station is extremely high (taking The Keynes IL laser displacement sensor as an example, its measurement accuracy can reach $10\mu m$ within the full range), it can be inferred that the measuring accuracy of the base station can also be controlled within 0.1mm.

Compared with the current commercial global measurement system: 1) Leica AT960, the measurement accuracy is $15\mu m + 6\mu m/m$, that is, within the measurement range of 10m, the maximum measurement uncertainty is 0.075mm; 2) Nikon iGPS system, the measurement accuracy is $0.2mm+10\mu m/m$, that is, within the measurement range of 10m, the maximum measurement uncertainty is 0.3mm. Therefore, the accuracy of the proposed measurement system is slightly better than the current commercial global large-space measurement equipment and can meet the calibration requirements of the AIMM.

B. CALIBRATION UNDER MEASUREMENT NOISE

In order to verify the proposed large-space on-line calibration method, we utilize the KUKA R500 manipulator with 0.08mm repetitive positioning accuracy to perform the calibration experiments. According to the complete kinematic modeling in section V, the parameters KN that need to be calibrated include three parts, $KN = \left[K_w^T \ K_r^T \ K_t^T \right]^T$.

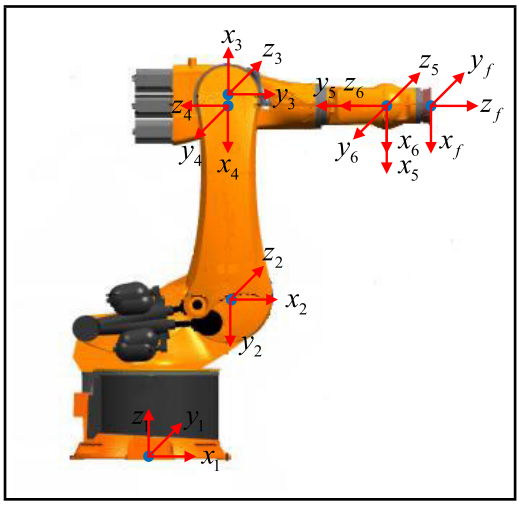

FIGURE 13. Kinematic model of the KUKA R500 manipulator.

TABLE 1. Nominal kinematic parameters of the KUKA R500 manipulator.

i	$\theta_i/(^\circ)$	$d_i/(mm)$	$a_i/(mm)$	$\alpha_i(^\circ)$	$\beta_i/(^\circ)$
1	0	1045	500	-90	0
2	-90	0	1300	0	$\beta_2 = 0$
3	180	0	55	-90	0
4	0	-1025	0	90	0
5	0	0	0	-90	0
6	0	-290	0	180	0

TABLE 2. Nominal parameters of world-manipulator frame and EE-flange frame.

	$\gamma_{xyz}/(^\circ)$	$d_{xyz}/(mm)$
${}^W_M T$	[0, 0, 35]	[3497.934, 4302.207, 520.342]
${}^F_E T$	–	[150, 120, 200]

1) The parameters for robot arm, which is expressed as $K_r = \left[\theta_1\ d_1\ a_1\ \alpha_1\ \ldots\ \theta_6\ d_6\ a_6\ \alpha_6\ \beta_2\right]^T$, and the labelled link coordinate systems and nominal geometric parameters are shown in Fig. 13 and Table 1, respectively.

2) The parameters to represent ${}^W_M T$, which includes 3 translation parameters and 3 rotation parameters $K_w = \left[{}^w d_x\ {}^w d_y\ {}^w d_z\ {}^w\gamma_x\ {}^w\gamma_y\ {}^w\gamma_z\right]^T$. The nominal values of K_w is given by the measurement data of IRAC, and expressed in the first row of Table 2.

3) The parameters to represent ${}^F_E T$, which includes 3 translation parameters $K_t = \left[{}^t d_x\ {}^t d_y\ {}^t d_z\right]^T$. The nominal values of K_t is designed by SolidWorks software, and expressed in the second row of Table 2.

The process of calibration experiment includes the following steps, and the flow chart is shown in Fig.14:

STEP 1 (Estimating the Robot Pose): In order to simulate the actual (theoretical) kinematic parameters of robot arm, we add a fixed bias to each nominal parameter. Due to the nominal values of d_i, a_i, α_i are given by robot manual, and we can obtain θ_i by reading simulated motor encoder. $\Delta\alpha_i$ is set randomly from normal random distribution with 0 average value and 0.1° standard deviation, Δd_i and Δa_i are set randomly from normal random distribution with 0 average value and 1 mm standard deviation. Then, we can generate groups (configurations) of actual position and orientation of EE base on the actual (theoretical) kinematic parameters.

STEP 2 (Data Measurement): Add the measurement noise into the actual pose of the end-effector. The measurement noise is gaussian noise with amplitude equals the maximum measurement uncertainty of measurement system. Several robotic measurement configurations are pre-defined, we adopt the poses of EE and corresponding joints angles with different robotic configurations.

STEP 3 (Kinematic Parameter Identification): Base on the kinematic model in section V, we use the measured data in STEP 2 to identify the robotic complete kinematic parameters. Because the proposed calibration method splits the identification process into two steps, STEP 3 will be executed several times. After we obtain the parameter errors ΔK, the nominal parameters will be updated by $KUP = KN + \Delta K$, where the KUP represents the calibrated parameter values. The results of calibrated parameter values compared with the actual parameter values are shown in Table 3. It's worth noting that the redundant parameters in the error model can be found through the analysis of identification matrix, which will lead to model singularity and reduce the effectiveness of parameter identification. The redundant parameters include all the inoperative parameters and some linearly dependent parameters. The inoperative parameters should be directly removed, while only independent parameters are reserved. For example, the corresponding column elements of $\Delta\theta_6$ in identification matrix are all zero, which means the parameters do not work and should be directly eliminated. The corresponding column of Δd_6 is linearly dependent with the column of $\Delta^e d_z$, and one of them has to be removed.

STEP 4 (Calibration Precision Evaluation): Take the cartesian distance RES_1 between the actual (theoretical) position and the nominal position as the positioning error before calibration,

$$RES_1 = \left\| {}^W_E p_a(k) - {}^W_E p_n(k) \right\| \tag{15}$$

and the cartesian distance RES_2 between the actual (theoretical) position and the calibrated position as the positioning error after calibration,

$$RES_2 = \left\| {}^W_E p_a(k) - {}^W_E p_{up}(k) \right\| \tag{16}$$

where k is the k-th measurement configuration. The ${}^W_E p_a(k)$ represents the actual (theoretical) position in the k-th measurement configuration, ${}^W_E p_n(k)$ and ${}^W_E p_{up}(k)$ represent the

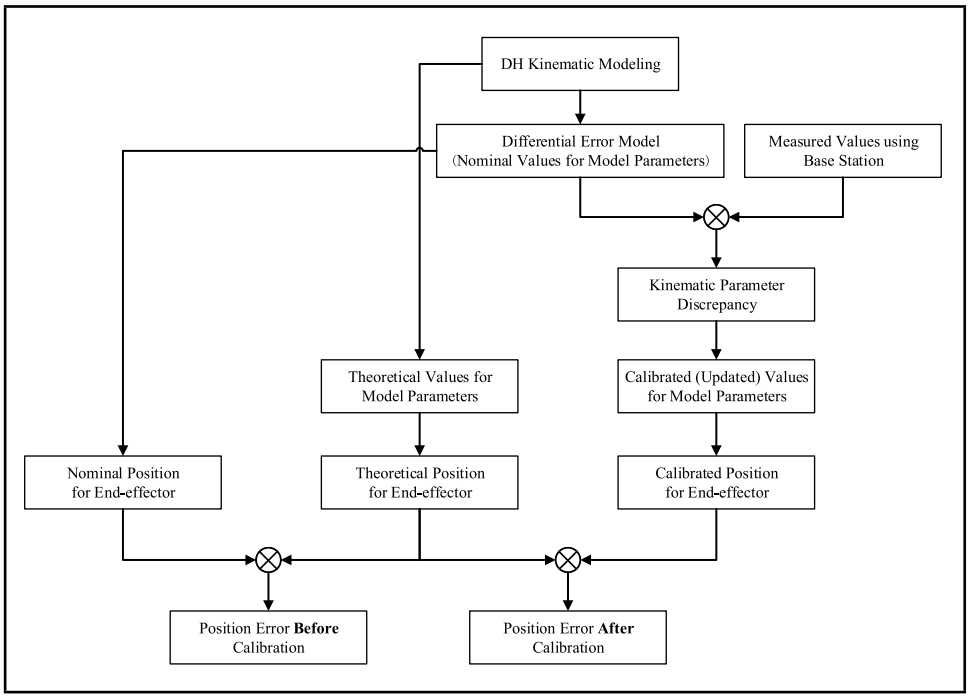

FIGURE 14. The calibration process of complete kinematic parameters.

TABLE 3. The theoretical parameters V.S. the calibrated parameters.

Items	Theoretical Value	Calibrated Value	Items	Theoretical Value	Calibrated Value
${}^{w}d_x$	3500	3499.660	a_3	55.108	55.1117
${}^{w}d_y$	4300	4299.713	d_3	0.096	0.0990
${}^{w}d_z$	520	–	θ_4	-0.026	-0.0254
${}^{w}\gamma_x$	0.023	0.0227	α_4	89.915	89.9147
${}^{w}\gamma_y$	0.006	0.0058	a_4	0.099	0.0981
${}^{w}\gamma_z$	34.985	34.9845	d_4	-1024.887	-1024.882
θ_1	-0.009	0.0032	θ_5	-0.041	-0.0408
α_1	-89.982	-89.9818	α_5	-89.960	-89.961
a_1	500.103	500.1026	a_5	0.098	0.0974
d_1	1045.092	1044.875	d_5	0.082	0.0756
θ_2	-90.045	-90.0453	θ_6	-0.063	–
α_2	-0.096	-0.096	α_6	180.069	180.3095
a_2	1300.097	1300.102	a_6	0.083	0.1850
d_2	0.101	–	d_6	-289.902	-290.2468
β_2	-0.294	-0.2936	${}^{e}d_x$	149.500	150.4850
θ_3	180.061	180.0615	${}^{e}d_y$	120.300	120.3781
α_3	-89.984	-89.984	${}^{e}d_z$	201.100	–

before calibrated position and after calibrated position of end-effector respectively. The average positioning errors, maximum positioning errors and standard deviation are counted in Table 4, and the before and after calibration position errors are detailed shown in Fig.15, where the blue dashed line represents RES_1 and green solid line represents RES_2.

The calibration experiment for KUKA R500 robot shows the result: before calibration, the maximum absolute positioning error, mean positioning error and standard deviation of the robot arm are 10.70mm, 4.96mm and 1.88mm, respectively; after calibration, the maximum absolute positioning error, mean positioning error and standard deviation

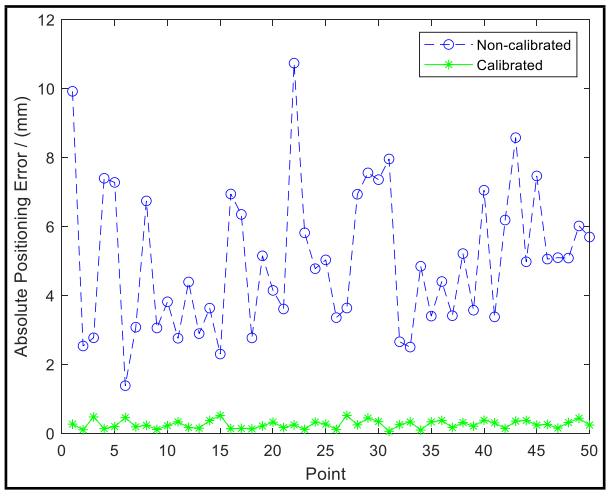

FIGURE 15. The position error of end-effector.

TABLE 4. Maximum error & Mean error & Standard deviation of error.

	$Max./(mm)$	$Mean/(mm)$	$Std./(mm)$
RES_1	10.695	4.958	1.8784
RES_2	0.630	0.316	0.140

of the robot arm were 0.63mm, 0.32mm and 0.14mm, respectively.

VII. CONCLUSION

In summary, the proposed solution by using multi-level measurement strategy to figure out the issue of the large-space localization and high-accuracy calibration of AIMM, which avoids the huge measurement cost using the global high-precision measuring equipment and the shielding problem in the actual industrial conditions. The result of experiment displays that the distributed short-range laser measurement possesses the accuracy within 0.1mm in 10m-level space, which is similar to the existing large-space measuring equipment. Therefore, the AIMM realizes spatial positioning and geometric error parameters calibration simultaneously. The mean positioning error of end-effector is less than 0.32mm, i.e. 93% lower compared with the mean positioning error with the non-calibrated situation.

When considering the measurement error of the measurement system, the kinematics parameter identification Jacobian matrix reflects the functional mapping relationship between the system measurement noise and the calibration residual. Since the Jacobian matrix is directly determined by measurement configuration, the robustness of the calibration parameter error is closely related to the selected measurement configuration, which is not covered in this paper. In the future work, the method of optimal choice for the measured configurations is going to be studied and analyzed for reducing the calibration residual even further.

REFERENCES

[1] H. Liu, W. Zhu, and Y. Ke, "Pose alignment of aircraft structures with distance sensors and CCD cameras," *Robot. Comput.-Integr. Manuf.*, vol. 48, pp. 30–38, Dec. 2017.
[2] K. Manohar, T. Hogan, J. Buttrick, A. G. Banerjee, J. N. Kutz, and S. L. Brunton, "Predicting shim gaps in aircraft assembly with machine learning and sparse sensing," *J. Manuf. Syst.*, vol. 48, pp. 87–95, Jul. 2018.
[3] R. Devlieg and T. Szallay, "Applied accurate robotic drilling for aircraft fuselage," *SAE Int. J. Aerosp.*, vol. 3, no. 1, pp. 180–186, Sep. 2010.
[4] B. Tao, X. Zhao, and H. Ding, "Mobile-robotic machining for large complex components: A review study," *Sci. China Technol. Sci.*, vol. 62, no. 8, pp. 1388–1400, Aug. 2019.
[5] M. Saadat and L. Cretin, "Measurement systems for large aerospace components," *Sensor Rev.*, vol. 22, no. 3, pp. 199–206, Sep. 2002.
[6] R. S. Andersen, J. S. Damgaard, O. Madsen, and T. B. Moeslund, "Fast calibration of industrial mobile robots to workstations using QR codes," in *Proc. IEEE ISR*, Oct. 2013, pp. 1–6.
[7] M. Shah, R. Bostelman, S. Legowik, and T. Hong, "Calibration of mobile manipulators using 2D positional features," *Measurement*, vol. 124, pp. 322–328, Aug. 2018.
[8] G. Wang, X. Liu, and S. Han, "A method of robot base frame calibration by using dual quaternion algebra," *IEEE Access*, vol. 6, pp. 74865–74873, 2018.
[9] G. Du, P. Zhang, and D. Li, "Online robot calibration based on hybrid sensors using Kalman filters," *Robot. Comput.-Integr. Manuf.*, vol. 31, pp. 91–100, Feb. 2015.
[10] C. Yu and J. Xi, "Simultaneous and on-line calibration of a robot-based inspecting system," *Robot. Comput.-Integr. Manuf.*, vol. 49, pp. 349–360, Feb. 2018.
[11] M. Hvilshøj, S. Bøgh, O. Skov Nielsen, and O. Madsen, "Autonomous industrial mobile manipulation (AIMM): Past, present and future," *Ind. Robot, Int. J.*, vol. 39, no. 2, pp. 120–135, Mar. 2012.
[12] S. Hayati and M. Mirmirani, "Improving the absolute positioning accuracy of robot manipulators," *J. Robot. Syst.*, vol. 2, no. 4, pp. 397–413, 1985.
[13] G. Chen, H. Wang, and Z. Lin, "Improving the absolute positioning accuracy of robot manipulators," *IEEE Trans. Robot.*, vol. 30, no. 5, pp. 1066–1077, May 2014.
[14] A. Nubiola and I. A. Bonev, "Absolute calibration of an ABB IRB 1600 robot using a laser tracker," *Robot. Comput.-Integr. Manuf.*, vol. 29, no. 1, pp. 236–245, Feb. 2013.
[15] G. Chen, T. Li, and S. Xu, "Review on kinematics calibration technology of serial robots," *Int. J. Precis. Eng. Manuf.*, vol. 15, no. 8, pp. 1759–1774, 2017.
[16] Y.-L. Kuo, B.-H. Liu, and C.-Y. Wu, "Pose determination of a robot manipulator based on monocular vision," *IEEE Access*, vol. 4, pp. 8454–8464, 2016.
[17] W. S. Newman, C. E. Birkhimer, and R. J. Horning, "Calibration of a Motoman P8 robot based on laser tracking," in *Proc. IEEE Int. Conf. Robot. Autom.*, vol. 4, Apr. 2000, pp. 3597–3602.
[18] H. N. Nguyen, J. Zhou, and H. J. Kang, "A calibration method for enhancing robot accuracy through integration of an extended Kalman filter algorithm and an artificial neural network," *Neurocomputing*, vol. 151, pp. 996–1005, Mar. 2015.
[19] A. M. Shafei and M. H. Korayem, "Theoretical and experimental study of dynamic load-carrying capacity for flexible robotic arms in point-to-point motion," *Optim. Control Appl. Methods*, vol. 38, no. 6, pp. 963–972, Nov. 2017.
[20] M. H. Korayem and H. Tourajizadeh, "Maximum DLCC of spatial cable robot for a predefined trajectory within the workspace using closed loop optimal control approach," *J. Intell. Robot. Syst.*, vol. 63, no. 1, pp. 75–99, Jul. 2011.
[21] C. Möller, H. C. Schmidt, P. Koch, C. Böhlmann, S.-M. Kothe, J. Wollnack, and W. Hintze, "Machining of large scaled CFRP-parts with mobile CNC-based robotic system in aerospace industry," *Procedia Manuf.*, vol. 14, pp. 17–29, 2017.
[22] S. Garnier, K. Subrin, P. Arevalo-Siles, G. Caverot, and B. Furet, "Mobile robot stability for complex tasks in naval industries," *Procedia CIRP*, vol. 72, pp. 297–302, 2018.
[23] A. R. Norman, A. Schönberg, I. A. Gorlach, and R. Schmitt, "Validation of iGPS as an external measurement system for cooperative robot positioning," *Int. J. Adv. Manuf. Technol.*, vol. 64, nos. 1–4, pp. 427–446, Jan. 2013.

[24] H. Susemihl, C. Moeller, S. Kothe, H. C. Schmidt, N. Shah, C. Brillinger, J. Wollnack, and W. Hintze, "High accuracy mobile robotic system for machining of large aircraft components," *SAE Int. J. Aerosp.*, vol. 9, no. 2, pp. 231–238, Sep. 2016.
[25] J. Borenstein, H. R. Everett, and L. Feng, *Navigating Mobile Robots: Systems and Techniques*. Wellesley, MA, USA: AK Peters, 1996.
[26] G. Du and P. Zhang, "Online serial manipulator calibration based on multisensory process via extended Kalman and particle filters," *IEEE Trans. Ind. Electron.*, vol. 61, no. 12, pp. 6852–6859, Dec. 2014.
[27] Q. Zhu, X. Xie, C. Li, G. Xia, and Q. Liu, "Kinematic self-calibration method for dual-manipulators based on optical axis constraint," *IEEE Access*, vol. 7, pp. 7768–7782, 2019.
[28] F. Franceschini, M. Galetto, D. Maisano, and L. Mastrogiacomo, "Large-scale dimensional metrology (LSDM): From tapes and theodolites to multi-sensor systems," *Int. J. Precis. Eng. Manuf.*, vol. 15, no. 8, pp. 1739–1758, Aug. 2014.
[29] T. Yang, Y. Pan, J. Mao, Y. Wang, and Z. Huang, "An automated optimization method for calibrating building energy simulation models with measured data: Orientation and a case study," *Appl. Energy*, vol. 179, pp. 1220–1231, Oct. 2016.
[30] Y. Yang, K. Deng, and M. Zhu, "Multi-level training and Bayesian optimization for economical hyperparameter optimization," 2020, *arXiv:2007.09953*. [Online]. Available: http://arxiv.org/abs/2007.09953
[31] G. N. Peggs, P. G. Maropoulos, E. B. Hughes, A. B. Forbes, S. Robson, M. Ziebart, and B. Muralikrishnan, "Recent developments in large-scale dimensional metrology," *Proc. Inst. Mech. Eng., B, J. Eng. Manuf.*, vol. 223, no. 6, pp. 571–595, Jun. 2009.
[32] T. Toshiyuki, K. Yoshihiko, and T. Yoshihisa, "Laser-tracking interferometer system based on trilateration and a restriction on the position of its laser trackers," *Proc. SPIE*, vol. 3479, pp. 319–326, Jul. 1998.
[33] A. Wan, J. Xu, D. Miao, and K. Chen, "An accurate point-based rigid registration method for laser tracker relocation," *IEEE Trans. Instrum. Meas.*, vol. 66, no. 2, pp. 254–262, Feb. 2017.
[34] R. Paul, *Robot Manipulators: Mathematics, Programming, and Control*. Cambridge, MA, USA: MIT Press, 1981.
[35] H. Zhuang, Z. S. Roth, and R. Sudhakar, "Simultaneous robot/world and tool/flange calibration by solving homogeneous transformation equations of the form AX=YB," *IEEE Trans. Robot. Autom.*, vol. 10, no. 4, pp. 549–554, Aug. 1994.

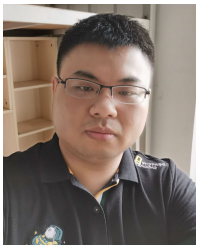

SHENG JIAN received the B.E. degree in automation from Central South University, Changsha, China, in 2013, and the M.E. degree in control science and engineering from the Harbin Institute of Technology, Shenzhen, China, in 2016, where he is currently pursuing the Ph.D. degree in control science and engineering. His research interests include robotics, industrial robot application, and calibration.

XIANSHENG YANG (Graduate Student Member, IEEE) received the B.E. degree in measurement and control technology and instrumentation from the Harbin Engineering University, Harbin, China, in 2012, and the M.E. degree in control science and engineering from the Harbin Institute of Technology, Shenzhen, China, in 2014, where he is currently pursuing the Ph.D. degree in control science and engineering. His research interests include robotics and 3D vision.

XIANWEI YUAN received the B.E. and M.E. degrees in mechanical engineering from the Harbin Institute of Technology, Harbin, China. He is currently pursuing the Ph.D. degree in control science and engineering with the Harbin Institute of Technology, Shenzhen, China.

YUNJIANG LOU (Senior Member, IEEE) received the B.S. and M.E. degrees in automation from the University of Science and Technology of China, Hefei, China, in 1997 and 2000, respectively, and the Ph.D. degree in electrical and electronic engineering from The Hong Kong University of Science and Technology, Hong Kong, in 2006. He is currently with the State Key Laboratory of Robotics and Systems, School of Mechatronics Engineering and Automation, Harbin Institute of Technology, Shenzhen, China, and the Shenzhen Key Lab for Advanced Motion Control and Modern Automation Equipments, Shenzhen. His research interests include motion control, mechanism design, and industrial robots.

YAO JIANG received the B.S. degree from the Nanjing University of Science and Technology (NUST), China, and the Ph.D. degree from Tsinghua University, in 2011 and 2016, respectively. He is currently an Assistant Researcher with the Department of Mechanical Engineering, Tsinghua University. His research interests include the intelligent robot, dexterous manipulator, grab, and collaboration robot.

GENLIANG CHEN (Member, IEEE) received the B.S. and Ph.D. degrees in mechanical engineering from Shanghai Jiao Tong University (SJTU), Shanghai, China, in 2006 and 2014, respectively. He is currently a Postdoctoral Researcher with the State Key Laboratory of Mechanical System and Vibration and the Shanghai Key Laboratory of Digital Manufacture for Thin-walled Structures, School of Mechanical Engineering, SJTU. His research interests include mechanism design, assembling automation, theoretical kinematics and dynamics, and robotics.

GUOYUAN LIANG (Member, IEEE) received the Ph.D. degree from the National Laboratory for Machine Perception (NLMP), Peking University, in 2005. From 2005 to 2006, he worked as a Research Assistant with the Advanced Robotic Laboratory, Department of Automation and Computer-Aided Engineering, The Chinese University of Hong Kong, where he is engaged with several projects related to video surveillance system and crowd modeling. He is currently an Associate Researcher with the Shenzhen Institutes of Advanced Technology, Chinese Academy of Sciences, and focus attention on medical image processing and digital vision technology.